Interpretation of neighboring group interactions in crystal structures. A solid state and quantum-chemical study of "incipient nucleophilic attack" in 2-diazonium benzoic acid and its benzoate[1]

Rainer Glaser and Christopher J. Horan

Abstract: The concept of the Bürgi–Dunitz angle of attack on carbonyls is compatible with the electronic structure of carbonyls. However, it is argued here that the generalization asserted to describe the interaction of nucleophiles with diazonium ions is inappropriate. Distortions in crystal structures of diazonium ions with proximate nucleophiles were interpreted by an incipient nucleophilic attack (INA) on the formally positive-charged N_α. This "N_α attraction model" relies on the assumption that the *formal* charge in the most commonly used Lewis structure of diazonium ions represents *actual* charge. We proposed that the close approach of the proximate nucleophile to the diazonium group occurs to enhance attractive 1,3-(C,N_β)-bridging interactions and despite repulsion between N_α and the proximate oxygen (O_{pr}). The present study combines theoretical analysis of rotamers of 2-diazonium benzoic acid and its conjugate base with experimental results *on the same system* to provide compelling evidence that the more general conclusions drawn from analyses of neighboring group interactions in propenoic acid models are fully warranted. The crystallographic record is more fully consistent with the "1,3-bridging attraction model." Combined analysis of solid state and gas phase structures reveals the intrinsic features due to INA. Both electrostatic models can account for these features but with different postulates about the electron density distribution. While the structural analysis alone cannot distinguish between the alternative interpretations, the study of the electronic structure allows one to clearly differentiate between these competing interpretations. A method (ESI) for the quantitative evaluation of electrostatic neighboring group interactions has been devised and this ESI concept employs atomic electrical moments (charges, dipoles, and quadrupoles) determined via topological electron density analysis. The results of the ESI analysis support the 1,3-bridging attraction model and eliminate the N_α attraction model.

Key words: electrostatic interactions, electron density analysis, atoms in molecules, X-ray crystallography, ab initio molecular orbital theory, incipient nucleophilic attack, bonding models, ESI analysis.

Résumé : Le concept de l'angle d'attaque sur les carbonyles de Bürgi–Dunitz est compatible avec la structure électronique des carbonyles. Il a toutefois été suggéré que la généralisation proposée pour décrire l'interaction des nucléophiles avec les ions diazonium est inappropriée. Les distorsions dans les structures cristallines des ions diazonium avec des nucléophiles à proximité ont été interprétées par une attaque nucléophile incidente (ANI) sur le N_α qui est formellement chargé positivement. Ce «modèle d'attraction N_α» se base sur l'hypothèse que la charge *formelle* dans la structure de Lewis la plus couramment utilisée pour les ions diazonium représente la charge *réelle*. Nous avons proposé que l'approche du nucléophile à faible proximité du groupe diazonium se produit pour augmenter les interactions attractives 1,3-(C,N_β) qui font le pont et malgré la répulsion entre le N_α et l'oxygène à proximité (O_{pr}). La présente étude combine une analyse théorique des rotamères de l'acide 2-diazoniumbenzoïque et de sa base conjuguée avec des résultats expérimentaux *sur le même système* qui fournit des données suggèrent fortement que les conclusions plus générales tirées de l'analyse des interactions des groupes avoisinants dans les modèles de l'acide propénoïque sont pleinement justifiées. Les données cristallographiques disponibles sont en meilleur accord avec le «modèle d'attraction à pont-1,3». Une analyse combinée des structures en phases solide et gazeuse met en relief les caractéristiques intrinsèques dues à l'ANI. Les deux modèles électrostatiques peuvent expliquer ces caractéristiques, mais en se basant sur des postulats différents concernant la distribution de la densité électronique. Même si l'analyse structurale seule ne permet pas de distinguer entre ces interprétations alternatives, l'étude de la structure électronique permet de bien différencier entre ces interprétations en compétition. La méthode (ESI) d'évaluation quantitative des interactions électrostatiques des groupes avoisinants a été mise au

Received October 19, 1995.

This paper is dedicated to Professor Richard F.W. Bader on the occasion of his 65th birthday.

R. Glaser[2] and C.J. Horan. Department of Chemistry, University of Missouri–Columbia, Columbia, MO 65211, U.S.A.

[1] Part 6 in the series "Incipient nucleophilic attack as a probe for the electronic structure of diazonium ions." For parts 1–5, see ref. 1*a–e*.

[2] Author to whom correspondence may be addressed. Telephone: (573) 882-0331. Fax: (573) 882-2754.
E-mail: chemrg@showme.missouri.edu

point et cette méthode fait appel aux moments électriques atomiques (charges, dipôles et quadripôles) déterminés par l'analyse de la densité électronique topologique. Les résultats de l'analyse ESI supportent le modèle d'attraction à pont-1,3 et permet d'éliminer le modèle d'attraction N_α.

Mots clés : interactions électrostatiques, analyse de la densité électronique, atomes dans les molécules, diffraction des rayons X, théorie des orbitales moléculaires ab initio, attaque nucléophile incidente, modèles de liaisons, analyse ESI.

[Traduit par la rédaction]

Scheme 1.

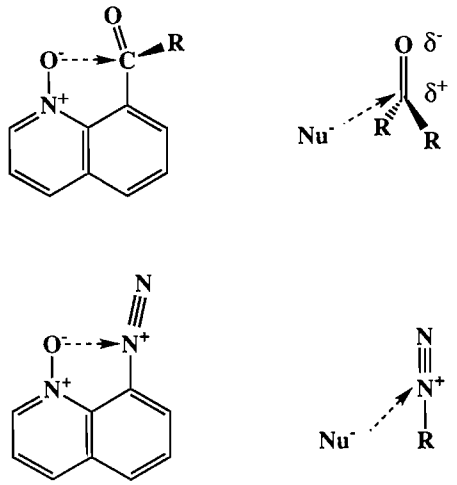

Scheme 2.

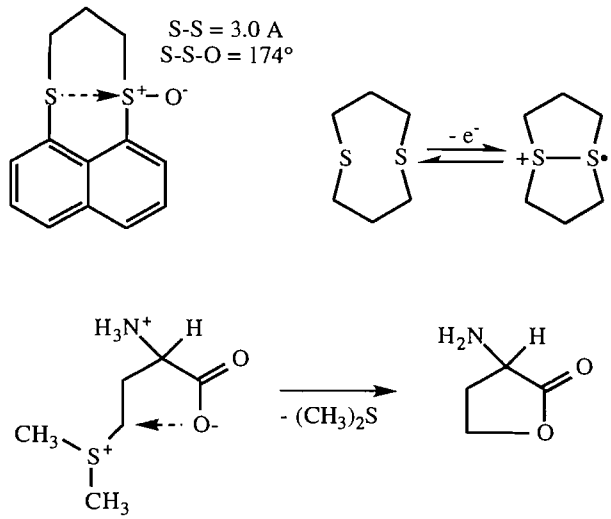

Introduction

The Bürgi–Dunitz angle of attack of a nucleophile on a carbonyl group was first described over 20 years ago (2), the feature was well established, and it is now "common knowledge." The trajectory of a nucleophile approaching a carbonyl in its π plane is not perpendicular but encloses an angle of 109° with the C=O σ-bond (Scheme 1). The angle of attack was determined both by a systematic analysis of crystal structures of compounds that contain either intra- or intermolecular nonbonded interactions between nucleophilic centers and carbonyl groups, and also by quantum-mechanical potential energy surface explorations. It was suggested that chemical reaction paths could be determined by examination of distortions in structural parameters caused by the presence of the two reactive centers in the "frozen" environment of the crystal lattice. Bürgi and Dunitz found the attack angle of 109° to be rather general for various nucleophiles and consistent distortions occurred for carbonyls in different environments. As the nucleophile's distance to the carbonyl decreased, the C=O distance increased and carbonyl C pyramidalization occurred. The idea of an "incipient nucleophilic attack" on a carbonyl center was demonstrated by Dunitz's elegant description of nucleophile–electrophile interactions in 1,8-disubstituted naphthalene and quinoline systems (3). In the seven systems studied, the distortions were consistent and characteristic of an initial nucleophilic attack. There was a splaying outward of the electrophilic carbonyl group and a splaying inward of the proximate nucleophile. The carbonyl carbon was also displaced toward the nucleophile and out of the plane of its three bonded atoms.

The Bürgi–Dunitz model for attack of nucleophiles on carbonyls is easily accepted as it is in agreement with the known electronic structure of carbonyls. The C=O bond is highly polar (4) for reasons of electronegativity and nucleophiles will be attracted to the electron-deficient carbonyl C. The nonperpendicular attack angle might be seen as a reflection of repulsive interactions between the nucleophile and the negatively charged carbonyl O. Because of its simplicity, this model quickly was applied to related systems as well. The attack of a nucleophile on a nitrile group can be discussed from this vantage point since the C≡N and C=O bonds show similar polarities (5). In fact, the concept of incipient nucleophilic attack has been broadened (6) to include not only nucleophilic attack on polar $^{\delta+}CX^{\delta-}$ or $^{\delta+}YO^{\delta-}$ multiple bonds but on all kinds of multiple bonds and to include dative bond formation as well.[3] In Scheme 2, a few examples of incipient nucleophilic attack on electron-deficient S centers are illustrated. The X-ray structure of the monosulfoxide suggests incipient sulfurane formation. The ease of oxidation of the disulfides was explained by incipient S—S bond formation (8). In a study of the directional preference of the approach of nucleophiles to sulfonium ions (9), 22 sulfonium ion crystal structures were analyzed for close contacts and interpreted as representing early stages of either an addition or a displacement reaction. Methylmethionine with its short C···O contact in the crystal exemplifies an early stage of facile conversion to a lactone.

Wallis and Dunitz asserted the generalization that an attack of a nucleophile on an NN triple bond will occur in a similiar fashion as with the carbonyls. Quinoline-8-diazonium-1-

[3] Intramolecular incipient nucleophilic attack on Si centers by aminoaryl groups: see ref. 7.

Scheme 3.

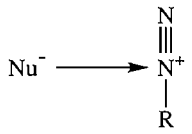

N_α attraction model

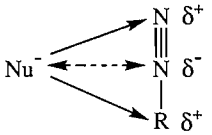

1,3-bridging attraction model

Scheme 4.

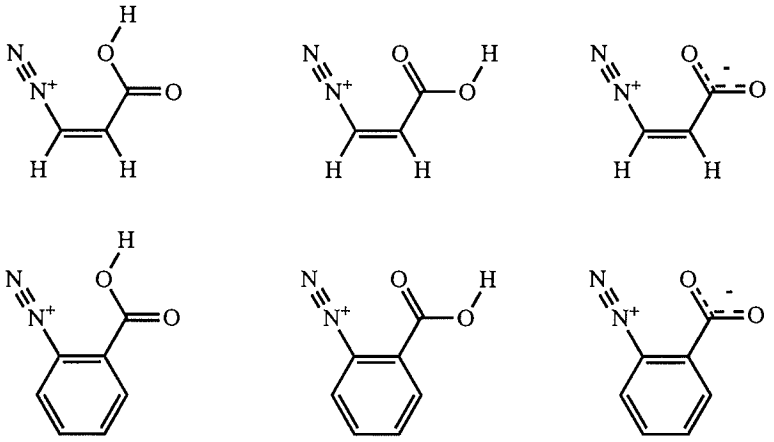

1 **2** **3**

oxide tetrafluoroborate (10) was discussed in complete analogy to the respective carbonyl system (Scheme 1) to argue that an incipient attack would occur at N_α (the central N). Several other cases of incipient nucleophilic attack on diazonium ions will be discussed below. This reasoning reflects the formal similarities of the Lewis structure (11) of diazonium ions with its formally positive-charged N_α and of the C=O bond polarity — this *formal* similarity is illustrated in a compelling fashion in Scheme 1. The explanation of distortions of diazonium ions by incipient nucleophilic attack relies on the assumption that N_α carries a positive charge and postulates an attractive interaction between the nucleophile and N_α (Scheme 3). Hence, this "N_α attraction model" would imply that the *formal* charge in the Lewis structure is a good representation of the *actual* charge distribution. Based on electronic structure analyses of diazonium ions, we argued that this assumption is not warranted and that the simple electrostatic model cannot be correct.

We proposed a bonding model for diazonium ions based on Bader's topological electron density analysis (12, 13) (TEDA) that emphasizes dative C←N bonding between a carbenium ion acceptor and an N_2 group donor that is internally polarized in the fashion $N_\alpha^{\delta-}$—$N_\beta^{\delta+}$ (14). This bonding model has since been shown to be general, fully consistent with all chemical and physical properties of diazonium ions,[4] and we argued for its preferability over purely formal bonding notations such as the Lewis notation (14*d*). In this context, we have been studying incipient nucleophilic attack in diazonium ions to probe their electronic structures. We first reported a theoretical study of neighboring group interactions in the rotamers of 3-diazonium propenoic acid and the zwitterionic conjugate base (1*a*). These systems were particularly suitable as they allowed for a variation of the nucleophilicity of the proximate O-atom (O_{pr}: C-O̲H, C=O̲, C-O̲$^-$) in the proximity of the N_2 group without major skeleton changes. Secondly, an aliphatic unsaturated molecule was selected because it allowed us to study the incipient nucleophilic attack in the *cis* isomer in comparison to the *trans* isomers as reference. We provided compelling evidence that the distortions occur in order to optimize the electrostatic interactions associated with the quadrupolar charge arrangement of the N_2 group and the C—O_{pr} bond. We showed that the close approach of the proximate nucleophile to the diazonium group occurs to enhance attractive 1,3-(C,N_β)-bridging interactions and *despite* N_α–O_{pr} *repulsion* (Scheme 3). We succeeded in the determination of the X-ray structures of the first β,β-disubstituted vinyldiazonium ions (16) but the synthesis and crystallization of β-*mono*substituted vinyldiazonium ions remain elusive. To corroborate our arguments, we thought it necessary to undertake a theoretical and experimental study on the *same* molecule and we resorted to aromatic diazonium systems. The crystal structures of 3-carboxy-2-naphthalenediazonium salt reported by Gougoutas and Johnson (17) were appealing but somewhat large from the viewpoint of computational demands. Hence, we focused on the *ortho*-carboxyl benzenediazonium ions and we report here on the interpretation of the distortions present in their quantum-mechanically determined gas phase structures and their experimental solid state structures. The three gas phase structures considered (Scheme 4) are the rotamer of 2-diazonio

[4] Excellent new monographs are available: see ref. 15.

Table 1. Total energies and vibrational zero-point energies.

		RHF/3-21G			RHF/6-31G*		
No.	Sym.	Energy	VZPE	NI	Energy	VZPE	NI
1	C_s	−523.389 019	77.57	0	−526.353 357	77.14	0
2	C_s	−523.391 896	77.54	0	−526.359 159	77.26	0
3	C_s	−522.966 332	68.55	0	−525.945 001	68.23	0

[a]Total energies in atomic units and vibrational zero-point energies (VZPE) in kcal/mol.
[b]Number of imaginary frequencies, NI.

benzoic acid in which the hydroxyl O is close to N_2, **1**, the other rotamer of this acid, **2**, and the conjugate base 2-diazonium benzoate zwitterion, **3**. We were able to determine the crystal structures of one rotamer of the benzoic acid derivative, the monohydrate of 2-carboxybenzenediazonium chloride (1*b*), **4**·Cl^-·H_2O, and of the conjugate base, the explosive 2-carboxylatobenzenediazonium ion hydrate (1*d*), **6**·H_2O. In addition, we solved the structure of **5**·Cl^-, which can be seen as the 1:1 complex between **4**·Cl^- and **6** (1*c*). The nucleophilicity of the proximate oxygen in **5** should be in between those of **4** and **6**. Details of the solid state structures were communicated (1*b–d*). With the theoretical data, we can now distinguish between intrinsic and packing-related distortions and probe the consistency of the competing explanations. While the structural analysis alone cannot distinguish between the alternative interpretations, a method for the quantitative evaluation of electrostatic neighboring group interactions has been devised for this purpose. The ESI concept employs atomic electrical moments determined via topological electron density analyses and the results of the ESI analysis do provide independent information that strongly supports the 1,3-bridging attraction model and eliminates the N_α attraction model.

Computational methods

Restricted Hartree–Fock (RHF) ab initio calculations were carried out on IBM RS-6000 systems with the program Gaussian92/DFT (18, 19) and electron density analyses were performed on Silicon Graphics Indigo workstations. Geometries were optimized in C_s symmetry and the Hessian matrices were computed analytically for each of the structures to confirm that an extremum had indeed been located and to characterize the stationary structures via the number of negative eigenvalues. Optimizations and vibrational analyses were performed with the basis sets 3-21G and 6-31G*. Total energies and vibrational zero-point energies of **1–3** are listed in Table 1 and their RHF/6-31G* geometries are listed in Table 2 together with the solid state structural data. The electronic structure analyses were performed at the RHF/6-31G* level. Topological and integrated properties were determined using various modules of the Proaim program (20). Graphical representations of the integrated atomic moments were generated with the program Dipoles.[5] The analysis of the electrostatic interactions between neighboring groups was performed with our program ESI[6] and the theoretical background will be discussed below.

Results and discussion

Incipient nucleophilic attack in crystal structures of diazonium ions

In crystal structures of salts of diazonium ions that contain a proximate nucleophile, the N_2 group is bent in a way that was interpreted as the result of *intramolecular* incipient nucleophilic attack on N_α. As with the interpretation of the structure of quinoline-8-diazonium-1-oxide tetrafluoroborate (vide supra), Gougoutas and Johnson (17) attributed distortions in 3-carboxy-2-naphthalenediazonium salts and the corresponding zwitterion **I** mainly to attractive interactions between N_α and the carbonyl O and also between N_β and the counterion. *Intermolecular* incipient nucleophilic attack of sulfonate O on N_α has been discussed for **II** (21). The close O–N_α contact might equally well be explained as the result of minimization of the distances between the sulfonate O and the atoms N_β and $C(N_2)$. The placement of nucleophiles in 1,3-bridging positions is common, and structures are known of several diazonium ions with polyfluoro anions in which the F atoms are placed successively in the two CNN bridging positions and, if both of these are occupied, in the proximity of N_β. The crystal structures of **III** (22) and **IV** (23) both contain F atoms in such bridging positions with nearly equal F–N_α and F–N_β distances. The crystal structure of $PhN_2^+BF_4^-$ (24), **V**, provides an excellent example for the placement of counterions in the proximity of both N_2 group nitrogens and this bridging was regarded as the result of electrostatic interactions of F with N_α and N_β. Haymore and coworkers (25) studied host–guest assemblies **VI** formed by 18-crown-6 ethers and diazonium ions and the crystal structure[7] showed the N_2 group inserted into the cavity of the crown ether such that each O atom assumes a 1,3-bridging position between N_β and C_{ipso}.[8]

[5] R. Glaser. Department of Chemistry, University of Missouri–Columbia, 1990.

[6] R. Glaser, B.S. Chladny, and M.K. Hall. Department of Chemistry, University of Missouri–Columbia, 1994.

[7] B.L. Haymore. Unpublished results. We thank Dr. Haymore for communicating these X-ray data prior to publication.

[8] Similar coordination of a 21-crown-7 ether to 4-methoxybenzene-1-diazonium cation also has been observed: ref 26.

Table 2. Comparison between computed gas-phase geometries and experimental solid state structures.

	Ab initio theory			X-ray crystallography		
Parameter	**1**	**2**	**3**	**4**	**5**	**6**
C1—N2	1.419	1.422	1.424	1.406(3)	1.415(4)	1.406(4)
N2—N3	1.075	1.075	1.075	1.085(3)	1.076(4)	1.090(3)
C1—C4	1.384	1.380	1.394	1.374(3)	1.384(4)	1.386(4)
C4—C5	1.385	1.387	1.373	1.373(4)	1.379(5)	1.376(4)
C5—C6	1.383	1.382	1.398	1.383(4)	1.371(5)	1.389(3)
C1—C7	1.401	1.400	1.382	1.397(3)	1.387(4)	1.398(2)
C6—C8	1.394	1.396	1.381	1.391(3)	1.389(5)	1.385(4)
C7—C8	1.379	1.378	1.390	1.378(3)	1.383(4)	1.387(4)
C7—C13	1.503	1.498	1.561	1.494(3)	1.494(4)	1.526(3)
C13—O14	1.177	1.189	1.231	1.208(3)	1.224(4)	1.250(3)
C13—O15	1.324	1.307	1.210	1.311(3)	1.280(4)	1.239(2)
C4—H9	1.074	1.074	1.074	0.79(3)	1.02(4)	0.95(2)
C5—H10	1.073	1.073	1.074	0.99(3)	1.01(4)	0.98(3)
C6—H11	1.074	1.074	1.075	0.88(3)	0.92(4)	0.98(3)
C8—H12	1.072	1.072	1.072	0.90(3)	0.94(4)	0.99(2)
O15—H16	0.957	0.956		0.99(3)	1.22(2)	
C1-N2-N3	176.89	176.62	170.42	173.3(3)	172.7(3)	174.29(16)
N2-C1-C7	120.86	120.06	119.17	119.49(19)	119.2(3)	118.54(23)
N2-C1-C4	114.70	115.42	115.12	115.64(21)	115.0(3)	116.06(17)
C1-C7-C13	126.11	120.62	121.34	120.98(17)	123.3(3)	122.27(24)
C8-C7-C13	117.86	122.98	123.17	123.07(20)	121.8(3)	122.72(15)
C7-C13-O14	122.59	121.69	111.51	121.40(20)	119.0(3)	115.91(15)
C7-C13-O15	112.61	112.86	114.51	112.69(17)	114.2(3)	115.75(19)
O14-C13-O15	124.80	125.50	133.98	125.85(20)	126.8(3)	128.33(21)
C4-C1-C7	124.44	124.51	125.71	124.78(19)	125.7(3)	125.3(3)
C1-C7-C8	116.02	116.40	115.49	115.87(19)	114.9(3)	115.01(22)
N2-C1-C7-C13	0.00	0.00	0.00	7.4(1)	7.0(2)	5.1(1)
C1-C7-C13-O14	180.00	0.00	0.00	12.3(1)	6.5(2)	25.9(1)
C1-C7-C13-O15	0.00	180.00	180.00	−170.5(2)	−176.2(4)	−154.3(3)

[a]Bond lengths in Å and bond angles and dihedrals in degrees.
[b]Estimated standard deviations are given in parentheses for the solid state data.
[c]Ab initio geometries determined at the RHF/6-31G* level.

Most recently, Wallis, Easton, and Dunitz (10*b*) reported the crystal structures of three 8-substituted naphthalene-1-diazonium ions, **VII**a, and the authors reiterated their previously stated view that the distortions are due to the attack of the electron-rich nucleophiles on the electron-deficient N_α. It was recognized that the functional groups are on opposite sides of the best molecular plane and this observation was said to be indicative of "attractive interactions between an electron-rich atom ... and the α-N atom of the diazonium group." In the earlier paper (10*a*) on the quinoline **VII**b, this feature was thought to disfavor their interpretation and downplayed as it "only increases the O(1)···N(1) separation by 0.017 Å." We pointed out (1*a*) that placing the two functional groups on opposite sides of the plane of the aromatic ring is *not* supportive of the suggested attractive interaction. In the crystal structure of 8-nitronaphthalene-1-diazonium ion, a system that is very closely related to the carboxyl-substituted structures, the NO_2 group is rotated out of the aromatic plane by 33°. This feature was said to assist in decreasing the distance between the nitro O and the diazonium α-N-atom. Certainly, rotating the nitro group out of the plane (and out of conjugation) only increases its distance from the N_2 group and this distortion is clearly not consistent and, in fact, is in contradiction to the idea of an attractive interaction between the nucleophile and N_α.

Neighboring group interactions in 2-diazonium benzoic acid derivatives

Crystal structures

The X-ray structures of the *ortho*-carboxy benzenediazonium ions **4–6** are shown in Fig. 2. Several types of distortions are pertinent to our discussion. The first two concern *in-plane deformations* of bond angles and specifically (*a*) the deviations from CNN linearity and (*b*) the splaying apart of the angles ∠(N_2-C═C) and ∠(C═C-CO_2). Two further types of distortions concern *out-of-plane displacements* of the functional groups and they include (*c*) the positioning of the two functional groups on opposite sides of the molecular plane and

Fig. 1. Examples of incipient nucleophilic attack in crystal structures of diazonium ions (charges on counterions omitted): 3-carboxylate-2-naphthalenediazonium zwitterion (**I**); 2-diazonium-4-phenolsulfonate monohydrate (**II**); *para*-bromobenzene tetrafluoroborate (**III**); *para*-diethylaminobenzenediazonium hexafluorophosphate (**IV**); benzenediazonium tetrafluoroborate (**V**); 18-crown-6 ether complexed benzenediazonium ion (**VI**); naphthalene-1-diazonium ions (**VII**a) and 8-substituted quinoline diazonium ions (**VII**b).

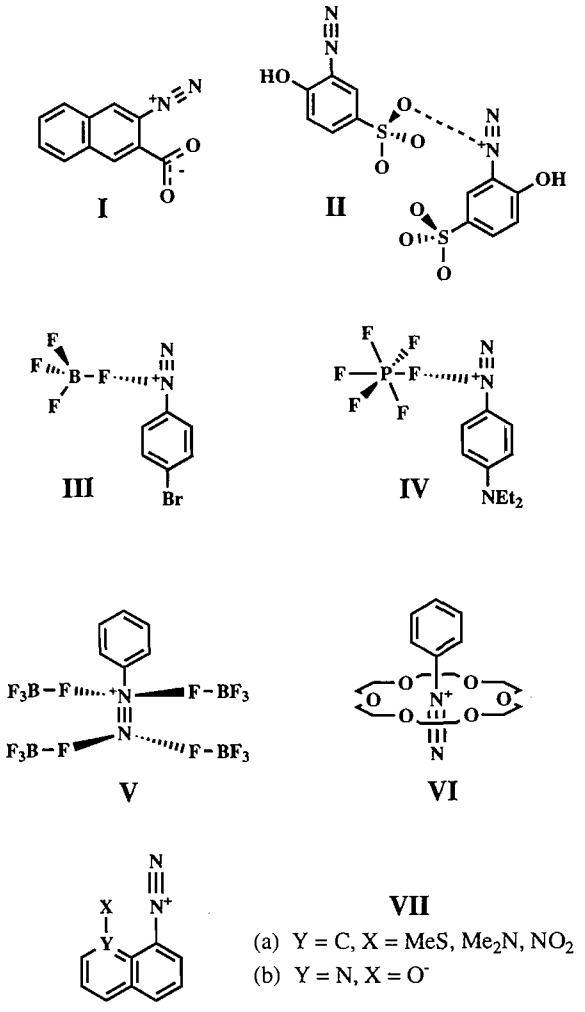

Fig. 2. Perspective view of the cations **4**–**6** contained in 2-carboxybenzenediazonium chloride monohydrate, $\mathbf{4}\cdot Cl^{-}\cdot H_2O$, in the symmetrically H-bridged system formed by 1:1 complex formation between 2-carboxybenzene-diazonium chloride and benzenediazonium-2-carboxylate, $\mathbf{5}Cl^{-}$, and in the 2-carboxylatobenzenediazonium ion hydrate, $\mathbf{6}^{-}H_2O$. Thermal ellipsoids are drawn at the 50% probability level.

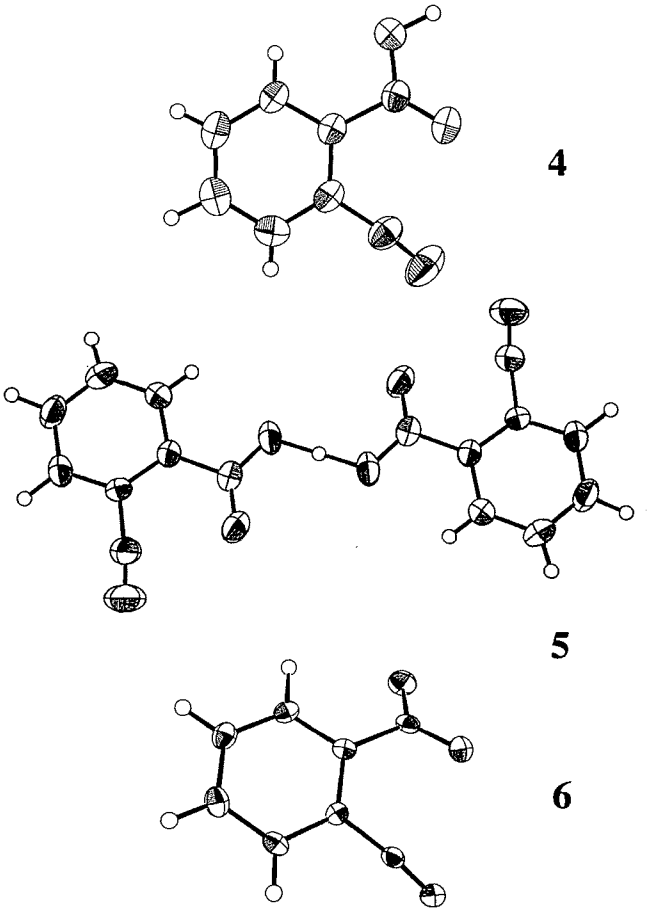

(*d*) the rotation of the carboxyl groups about the C(7)—C(13) bonds.

Primarily, the in-plane deformations were considered as evidence for an attraction between O_{pr} and N_{α}. In **4**–**6**, N_{β} is displaced away from the carboxyl group resulting in deviations of the C(1)-N_{α}-N_{β} skeleton from linearity by 5–7°. Benzenediazonium ions are well known to exhibit widened C-C_{ipso}-C angles at the N_2 bearing C atom (1*c*). It is because of *this* effect on the C(4)-C(1)-C(7) angles (>124.8°) that the other angles at C(1) have to be less than 120°. We find the angles N(2)-C(1)-C(4) and N(2)-C(1)-C(7) to be about 115° and 119°, respectively, and they differ in a way that would position N_{α} *further away* from O_{pr}. The C(1)=C(7)-C(13) angles all are larger than the sp^2 angle of 120°. Hence, considering all of the crystallographic evidence, the in-plane deformations of the angles N(2)-C(1)-C(7) and C(1)-C(7)-C(13) certainly do not allow one to argue in favor of an attraction of O_{pr} to N_{α} but these angle widenings would increase the distance between the two neighboring groups.

The N_2 groups and the carboxyl groups are on opposite sides with regard to the best molecular plane with N(2)-C(1)-C(7)-C(13) dihedral angles of 7.4–5.1° for **4**–**6**. This displacement increases the N_{α}–O_{pr} distance. Another significant dihedral angle describes the carboxyl group rotation out of the plane of the aromatic ring and its value can be as high as 25.9°. These rotational distortions are due to *intermolecular* interactions and, in any case, it is clear that the rotational distortions certainly cannot be interpreted as evidence of N_{α}–O_{pr} attraction since O_{pr} is rotated *away* from the N_2 group.

Fig. 3. Molecular models of the RHF/6-31G* optimized planar minimum structures of **1–3** with integrated atomic charges.

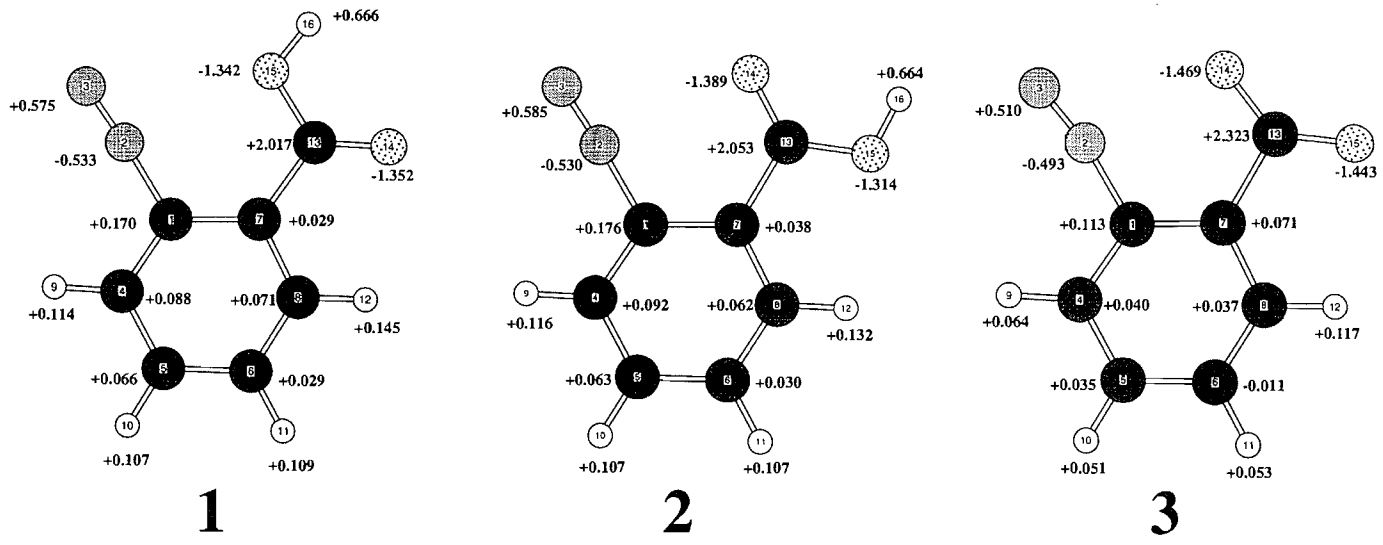

Calculated gas phase geometries

All the optimized planar structures **1–3** are minima[9] (Table 1 and Fig. 3) and we conclude that the out-of-plane distortions for **4–6** are due to packing. Basis set effects on structures are minimal, the agreement between theory and experiment is excellent, and, moreover, corresponding bond lengths in **1–3** differ only slightly (Table 2). The significant in-plane deformations found in **4–6** also occur in **1–3** (Table 2). The C(1)-N_α-N_β backbones are not linear (177° for **1** and **2**, 170.4° for **3**), there is a slight widening of the C(4)-C(1)-C(7) angles to values >124°, and the C(1)-C(7)-C(8) angles of 115.0°±0.5° are larger than in the parent benzenediazonium ion.

Intrinsic INA features and their interpretations

The combined analysis of the solid state and of the gas phase structural data shows that the intrinsic features associated with incipient nucleophilic attack on diazonium ions are the CNN nonlinearity and the widening of the in-plane angles. These features result in the nonbonded distances summarized in Table 3 and we note that the N_α–O_{pr} distances in all systems remain substantially less than the sum of the van-der-Waals radii of N and O (2.9 Å). Both the N_α attraction model and the 1,3-bridging attraction model account for these features with different postulates concerning the electron density distribution. The former explains the kink in the CNN backbone and the short N_α–O_{pr} contact with an attraction of the nucleophile to the positively charged N_α atom. The 1,3-bridging attraction model differs fundamentally in that it reflects the polarity $C(+)N(^{\delta-})N(^{\delta+})$ and it is slightly more complicated as it considers not just the interaction between O_{pr} and N_α, which is repulsive in this model. The C—O_{pr} and N_α—N_β bonds are arranged in a nearly perfectly aligned quadrupolar arrangement with roughly identical N_α–C and N_β–O_{pr} distances. The short N_α–O_{pr} distance results from the optimization of the 1,3-bridging O_{pr}–N_β and O_{pr}–C(N) attractions and N_α–C(O_{pr}) attraction as well. Note that the latter interaction provides a straightforward explanation of the kink in the CNN backbone. It is evident that *the structural characteristics can be interpreted based on different assumptions concerning the electronic structures*. A corollary statement would be that structure distortions *alone* do not allow one to make any deductions concerning electron density distribution. On the other hand, the study of the electronic structure will allow one to clearly differentiate between competing interpretation of the structural distortions.

Quantitative evaluation of electrostatic neighboring group interactions

AIM and the ESI concept

Both the N_α attraction model and the 1,3-bridging attraction model are electrostatic in nature. To formulate these models in quantitative terms, one needs to assign electrostatic moments to the atoms and evaluate their interactions. The concept of "atomic charge" is of paramount importance in discussions of all aspects of chemistry and many methods have been proposed to partition molecules into atoms and to assign charges to the atoms. Basis set partitioning and density partitioning methods have been developed (27). To the class of basis set partitioning methods belong, for example, the historically significant Mulliken population analysis and the modern Natural Population Analysis (28). The density partitioning methods do not rely on properties of the Hilbert space but consider directly the observable molecular electron density distribution in Cartesian space. As far as the partitioning of the molecular electron density distribution into atomic components is concerned, two schools of thought seek to recover either "spatially

[9] The conformational preference energy of 3.6 kcal/mol in favor of **2** compared to **1** is nearly the same as for the respective propenoic acid derivatives (3.8 kcal/mol). The proton affinity of 259.9 kcal/mol of **3**, however, is significantly higher than the value of 238.5 kcal/mol (ref. 1*a*) obtained at the same level for the aliphatic system.

Table 3. Theoretical and experimental nonbonded intramolecular interactions.

	Proximate oxygen, O_{pr}			Carboxyl carbon		
No.	C(1)	N_α	N_β	C(1)	N_α	N_β
1	2.839	2.586	2.938	2.589	3.015	3.725
2	2.842	2.575	2.923	2.518	2.876	3.567
3	2.731	2.396	2.826	2.566	2.889	3.639
4	2.855	2.603	3.013	2.516	2.864	3.600
5	2.851	2.594	3.006	2.535	2.901	3.640
6	2.866	2.622	3.020	2.561	2.887	3.600

[a]All values in Å.

extended" or "spatially constrained" atom-shaped objects. The approaches by Parr (29) and by Walker and Mezey (30) exemplify the former and Bader's topological Atoms in Molecules theory (12, 13) (AIM) is the most rigorous formulation of the latter. For the discussion of the majority of chemical problems, the AIM method is especially well suited and its widespread usage emphasizes this point. An aspect of the topological electron density analysis (TEDA) that is particularly appealing concerns its ability to deal with atom anisotropies (31, 32). Many population analyses merely describe atomic charges and few attempts have been made to include higher moments (33). For example, the extended Mulliken electron population analysis proposed by Huzinaga et al. produces a point charge model that correctly reproduces the molecular electric dipole moment (34). There have also been reports on the extensions of the Mulliken population analysis to include atomic polarizations to recover the molecular dipole moment.[10] The topological method allows for a more refined representation of the atom in a molecule since not only the charge but higher atomic moments as well can be determined. We will be interested in charges, dipoles, and quadrupoles of the atoms but still higher moments can also be determined.

Arguments based on charges and electrical moments can become rather involved as many values "with direction" need to be considered. It is thus important to define and discuss parameters that incorporate all of this information. As the basis for such parameters, we are studying the electrostatic interaction energy[11] between atoms i and j, ESI_{ij}, defined by the equation

$$ESI_{ij} = CC_{ij} + CD_{ij} + DD_{ij} + QC_{ij} + QD_{ij} + QQ_{ij}$$

where CC_{ij} is the Coulomb energy between the atomic charges q_i and q_j, CD_{ij} is the sum of the energies associated with the interaction of q_i with atomic dipole μ_j and of q_j with μ_i, and DD_{ij} is the interaction energy between the dipoles μ_i and μ_j. The remaining terms consider the interactions of the atomic quadrupoles with the charges (QC_{ij}), dipoles (QD_{ij}), and quadrupoles (QQ_{ij}).

Topological analysis and determination of electrical moments

The quantitative evaluation of electrostatic neighboring group effects[12] requires knowledge of the ESI_{ij} values, which in turn depend on the atomic properties evaluated by the AIM theory. We have determined all of the topological and integrated atomic properties and pertinent results are summarized in Tables 4 and 5. The analysis begins with the characterization of topological features of the electron density distribution based on the properties of the gradient vector field. The collection of all gradient vector field lines originating at a given atom, the attractor, define the associated zero-flux surfaces as the boundaries of the atoms in the molecules. Bond critical points occur at the intersection between the zero-flux surfaces and the so-called bond paths. A bond path connects two attractors and is defined as the line traced out by following the direction of positive curvature of the electron density (λ_3) beginning at the bond critical point. *In praxis*, one first locates all bond critical points and then traces out the zero-flux surfaces following the directions associated with the two negative principal curvatures of the density, λ_1 and λ_2. Properties of the bond critical points, such as the density at that point, ρ_b, and its distances r_A and r_B from the atoms, are commonly used to characterize electron density distributions and such information is collected in Table 4 for **1–3**. With the atomic regions defined, atomic properties are determined by numerical integration within the basins and this aspect is the most time-consuming step (36). Integrated properties are summarized in Table 5 and include the atomic charge and dipole moments. The directions of the dipole moments are shown in Fig. 4. The atomic quadrupole moments also were determined and employed in the ESI_{ij} evaluations but, for brevity, they are not documented.

Analysis of the data presented in Tables 4 and 5 shows the great similarity of the electronic structures of **1–3** and the respective propenoic acid derivatives. In fact, the electronic structures of aromatic and aliphatic diazonium functions are rather general (14). The N_α basins extend greatly into the C—N bonding region ($F_{CN} \approx 0.31$) and modestly ($F_{N\alpha N\beta} \approx 0.56$) into the N—N bonding region. Fairly typical ρ_b values of about 0.22 and 0.68 are found for all of the C—N and N—N bond critical points. Negative N_α charges in the range from -0.53 to -0.49 are found for **1–3** and the N_β charges are positive, just slightly larger in magnitude, and in the range between +0.51 and +0.58 (Fig. 3). Hence, the N_2 groups exhibit a large internal polarization but only a modest overall charge (< +0.055). The N_2 group polarization and the dative N→C bonding are manifested in the atomic moments of **1–3**. The vector $\mu(N_\alpha)$ is directed toward N_β and the $\mu(N_\beta)$ vector is antiparallel and much larger, and $\mu(C1)$ is directed toward N_α. The electron density within the basins of N_α and N_β is

[10] Compare the discussion of ethylene in ref. 32*b*.

[11] A similar approach was described by Cooper and Stutchbury in their study of hydrogen-bonded van de Waals complexes (35).

[12] Penetration effects are neglected in the present discussion. We found that the electron density between nonbonded atoms provides a good indication for assessing the importance of penetration effects. If the electron density is as low as in the present cases (between N_α and O_{pr}), then the neglect of penetration effects is warranted to a first approximation even though the N_α–O_{pr} distance is less than the sum of the van der Waals radii. One has to keep in mind that the sum of the van der Waals radii provides only a rather crude parameter for the assessment of steric effects because the van der Waals radius of an "N_α in a diazonium ion" is different from "the van der Waals radius of prototypical N" and so forth.

Table 4. Topological characteristics of bond and ring critical points of the electron densities.[a]

No.	A	B	r_A	r_B	F	ρ_b	λ_1	λ_2	λ_3	ε
Molecule 1										
1	C1	N2	0.434	0.984	0.306	0.220	−0.306	−0.258	1.222	0.185
2	N2	N3	0.604	0.471	0.562	0.680	−1.545	−1.512	0.430	0.022
3	C1	C4	0.761	0.623	0.550	0.326	−0.709	−0.564	0.211	0.257
6	C1	C7	0.764	0.637	0.545	0.314	−0.673	−0.539	0.234	0.247
8	C7	C8	0.727	0.651	0.528	0.331	−0.716	−0.584	0.248	0.226
13	C7	C13	0.752	0.751	0.500	0.277	−0.594	−0.542	0.317	0.097
14	C13	O14	0.422	0.902	0.318	0.317	−0.823	−0.777	1.503	0.060
15	C13	O15	0.386	0.791	0.328	0.451	−1.374	−1.200	3.119	0.145
16	O15	H16	0.783	0.172	0.820	0.347	−1.909	−1.882	1.646	0.014
17	N2	O15	1.268	1.323	0.489	0.016	−0.015	−0.013	0.099	0.089
18[b]	C1	C6	1.323	1.390	0.488	0.020	−0.014	0.086	0.095	
19[c]	C1	O15	1.498	1.376	0.521	0.013	−0.009	0.024	0.061	
Molecule 2										
1	C1	N2	0.435	0.986	0.306	0.220	−0.308	−0.267	1.193	0.153
2	N2	N3	0.603	0.471	0.561	0.681	−1.543	−1.520	0.430	0.016
3	C1	C4	0.759	0.621	0.550	0.329	−0.715	−0.567	0.209	0.261
6	C1	C7	0.764	0.637	0.545	0.316	−0.681	−0.545	0.233	0.250
8	C7	C8	0.724	0.653	0.526	0.332	−0.717	−0.582	0.250	0.231
13	C7	C13	0.746	0.751	0.498	0.281	−0.606	−0.553	0.318	0.097
14	C13	O14	0.388	0.800	0.326	0.441	−1.332	−1.194	2.952	0.116
15	C13	O15	0.417	0.890	0.319	0.333	−0.891	−0.854	1.642	0.043
16	O15	H16	0.782	0.173	0.819	0.349	−1.916	−1.890	1.657	0.013
17	N2	O14	1.247	1.333	0.483	0.018	−0.018	−0.016	0.110	0.148
18[b]	C1	C6	1.322	1.388	0.488	0.020	−0.014	0.087	0.095	
19[c]	C1	O14	1.463	1.414	0.508	0.015	−0.012	0.028	0.073	
Molecule 3										
1	C1	N2	0.436	0.988	0.306	0.218	−0.297	−0.256	1.173	0.162
2	N2	N3	0.607	0.467	0.565	0.681	−1.520	−1.516	0.409	0.002
3	C1	C4	0.748	0.646	0.536	0.320	−0.694	−0.554	0.242	0.254
6	C1	C7	0.783	0.598	0.567	0.327	−0.687	−0.584	0.169	0.175
8	C7	C8	0.714	0.676	0.514	0.327	−0.698	−0.598	0.270	0.168
13	C7	C13	0.877	0.683	0.562	0.242	−0.491	−0.467	0.284	0.050
14	C13	O14	0.399	0.831	0.325	0.402	−1.159	−1.089	2.304	0.063
15	C13	O15	0.394	0.815	0.326	0.420	−1.239	−1.135	2.584	0.091
16	N2	O14	1.142	1.254	0.477	0.028	−0.030	−0.028	0.172	0.041
17[b]	C1	C6	1.318	1.375	0.489	0.021	−0.014	0.087	0.097	
18[c]	C1	O15	1.372	1.367	0.501	0.019	−0.015	0.043	0.090	

[a]Distances r_A and r_B in Ångstroms between each critical point and atoms A and B, respectively. F is defined as $F = r_A/(r_A + r_B)$. The electron density at the critical point, ρ_b, is given in e au^{-3}. The curvatures of the electron density at the locations of the critical points, λ_i, are given in e au^{-5}. The ellipticity, ε, is defined as $\varepsilon = \lambda_1/\lambda_2 - 1$ and given for all (3,+1) bond critical points.

[b]The locations of (3,−1) ring critical points within the benzene rings are characterized with respect to C1, the carbon that carries the diazonio function, and the "*para*-carbon".

[c]The locations of (3,−1) ring critical points between functional groups are characterized with respect to C1, the carbon that carries the diazonio function, and the proximate O14 or O15.

polarized into the CN bonding and the lone pair regions, respectively. The -CO_2H groups show large $q(C) \approx +2$, negative OH charges of about −0.66, and carbonyl-O charges of −1.39 (**1**) and −1.34 (**2**) that are more than twice as high. Since the acidic hydrogens carry positive charges of 0.66 in **1** and **2**, deprotonation adds only 0.34 electron to the fragment [$N_2C_6H_4CO_2$]. Since the electron populations of the CO_2 groups *decrease* from −0.68 and −0.65 in **1** and **2**, respectively, to −0.59 in **3** and since $q(N_2)$ remains indifferent, it follows that *deprotonation serves to reduce the electron deficiency in the phenyl ring*. This is quite a remarkable result: In the absence of the proton, it is no longer beneficial to accu-

Table 5. Integrated atomic charges (q), magnitude of the first atomic moments (μ), and atom stabilities (KE).

	1			2			3		
Atom	q	μ	KE	q	μ	KE	q	μ	KE
C1	+0.170	0.741	37.737 39	+0.176	0.748	37.742 26	+0.113	0.788	37.790 47
N2	−0.533	0.348	55.008 34	−0.530	0.348	55.002 07	−0.493	0.357	54.958 77
N3	+0.575	0.888	53.925 56	+0.585	0.887	53.919 74	+0.510	0.923	53.957 49
C4	+0.088	0.354	37.843 25	+0.092	0.352	37.840 16	+0.040	0.285	37.855 07
C5	+0.066	0.222	37.848 29	+0.063	0.218	37.847 46	+0.035	0.178	37.844 71
C6	+0.029	0.134	37.872 87	+0.030	0.133	37.870 26	−0.011	0.097	37.880 57
C7	+0.029	0.356	37.871 80	+0.037	0.394	37.874 30	+0.071	0.553	37.896 11
C8	+0.071	0.256	37.859 44	+0.062	0.242	37.856 63	+0.037	0.193	37.864 62
H9	+0.114	0.125	0.572 76	+0.116	0.125	0.571 70	+0.064	0.130	0.593 96
H10	+0.107	0.126	0.576 30	+0.107	0.126	0.576 48	+0.051	0.131	0.599 97
H11	+0.109	0.125	0.576 80	+0.107	0.126	0.577 68	+0.053	0.131	0.600 63
H12	+0.145	0.121	0.562 25	+0.132	0.120	0.569 24	+0.117	0.128	0.572 80
C13	+2.017	0.770	36.478 83	+2.053	0.792	36.480 30	+2.323	0.494	36.266 92
O14	−1.342	0.367	75.616 75	−1.389	0.734	75.701 91	−1.469	0.579	75.629 90
O15	−1.352	0.776	75.693 88	−1.314	0.408	75.619 88	−1.443	0.651	75.632 54
H16	+0.666	0.130	0.302 83	+0.663	0.130	0.305 97			
Σ	+0.959		526.347 34	+0.990		526.356 04	−0.002		525.944 53
C_6H_4	+0.928		229.321 15	+0.922		229.326 17	+0.570		229.498 91
N_2	+0.042		108.933 90	+0.055		108.921 81	+0.017		108.916 26
COOH	−0.011		188.092 29	+0.013		188.108 06	−0.589		187.529 36

[a]Deviation between directly calculated molecular energy and the sum over the negative atom kinetic energies (in kcal/mol): 3.77 for **1**, 1.96 for **2**, and 0.29 for **3**.

mulate as much excess density on the CO_2 fragments, and the CO_2 population and the charge on the phenyl ring are both reduced drastically. While the CO_2 population is reduced in **3**, the data in Table 5 also indicate a higher polarization, and the negative charges on O_{pr} (a measure of their nucleophilicity) increase in the order −1.34, −1.39, and −1.47 in going from **1** to **3**. The μ vectors of the carboxyl C-atoms all are more or less parallel to the C—CO_2 bond and directed into the region between the oxygens, and the μ vectors of the carbonyl and carboxylate oxygens are directed away from the carboxyl C. Note that the dipoles $\mu(N_\beta)$ and $\mu(O_{pr})$ are large and antiparallel whereas the dipoles $\mu(N_\alpha)$ and $\mu(O_{pr})$ are parallel to each other.

The similarities and differences between the electronic structures of the aromatic systems **1–3** and of the aliphatic propenoic acid derivatives come clearly to the fore. The electronic structures of the functional groups are very similar and the only significant difference lies with the assignment of positive charge to the hydrocarbon fragments C_6H_4 and C_2H_2 in the two series. While the positive charge necessarily remains local in the C_2H_2 groups, the positive charge is well dispersed in the phenyl groups.

Electrostatic interaction analysis

We determined the interaction terms for **1–3**, and in Tables 6–8 are listed the various electrostatic contributions due to each pair of atoms within the two functional groups together with their sum $\Sigma = ESI_{ij}$. These ESI_{ij} values are shown in Fig. 4. Most importantly, *this analysis provides compelling evidence that the more general conclusions we drew from our analyses of the neighboring group interactions in the propenoic acid models are fully warranted and completely corroborated by the present combined experimental and theoretical studies*. The interaction between N_α and the proximate oxygen nucleophile is repulsive. Strong 1,3-bridging attractions occur between N_β and O_{pr} and C(1) and O_{pr}. It is for these two statements that the interpretation based on the 1,3-bridging attraction model is consistent with the electronic structure while the N_α attraction model is eliminated. At the same time, one also must realize that *every* model presents a simplification. The 1,3-bridging attraction model does describe the dominant interactions in **II–VI**. However, Fig. 4 shows that there are other interactions between the neighboring groups that are quite large and that suggest that one needs to consider the bridging interactions not just of O_{pr} but also of the highly electron-deficient carboxyl-C atom with the atoms of the C-N-N fragment. Substantial repulsions occur between the carboxyl C and N_β and C(1) while there is strong attraction between N_α and the carboxyl C. The overall electrostatic interactions between O_{pr} with C(1) and the N-atoms are −42.0, −48.0, and −34.3 kcal/mol for **1–3**, respectively. The interactions of the carboxyl C with the CNN fragment are +37.1, +47.1, and +21.5 kcal/mol, respectively, for **1–3**. Two observations are noteworthy: The interaction between O_{pr} and the neighboring group is attractive in all cases but it does not parallel O_{pr} nucleophilicity and, similiarly, the interactions of the carboxyl C with the neighboring group all are repulsive but also do not parallel the charge on the carboxyl C. This observation reflects

Table 6. Electrostatic interaction matrix for **1**.

		N2	N3	C7	C13	O14	O15	H16
CC	C1	−21.1	13.0	1.2	43.9	−26.6	−20.9	9.9
CD		−39.5	16.3	4.4	−3.5	−9.8	0.7	2.9
CQ		12.5	−3.1	−2.6	−1.5	1.2	0.4	−0.3
DD		−8.3	3.9	−4.1	0.0	0.1	0.2	0.1
DQ		−4.1	3.6	−1.1	−0.3	0.2	−0.1	0.0
QQ		2.3	0.2	1.8	0.0	0.0	0.0	0.0
Σ		−58.3	34.0	−0.4	38.6	−35.0	−19.7	12.7
CC	N2		−94.6	−2.1	−118.3	91.8	57.1	−33.9
CD			−41.8	−5.5	−0.2	−3.4	6.1	−0.5
CQ			3.8	1.1	0.1	0.2	0.1	0.0
DD			22.8	−0.6	0.2	0.0	0.1	0.0
DQ			33.8	−0.1	−0.1	0.0	0.0	0.0
QQ			3.9	0.0	0.0	0.0	0.0	0.0
Σ			−72.1	−7.3	−118.3	88.5	63.4	−34.4
CC	N3			1.6	103.5	−87.3	−52.9	34.7
CD				3.1	14.5	−8.8	−9.7	3.4
CQ				−0.4	−0.8	−0.1	0.1	0.1
DD				0.6	−0.4	0.5	−0.4	0.1
DQ				0.4	0.1	0.0	0.0	0.0
QQ				0.0	0.0	0.0	0.0	0.0
Σ				5.3	116.8	−95.6	−62.9	38.3
CC	C7				13.0	−5.5	−5.6	2.0
CD					−24.1	−2.2	10.8	−0.1
CQ					−22.1	3.1	4.1	0.7
DD					3.0	0.0	1.2	0.0
DQ					−8.6	−0.2	−1.4	0.1
QQ					−0.3	0.0	0.0	0.0
Σ					−39.0	−4.8	9.2	1.3
CC	C13					−678.7	−769.5	238.0
CD						−91.3	−282.2	27.9
CQ						9.5	14.6	−0.6
DD						−2.6	−21.6	0.7
DQ						−3.4	−12.9	0.1
QQ						0.3	0.2	0.0
Σ						−766.2	−1071.3	266.1
CC	O14						271.6	−310.5
CD							50.0	−43.3
CQ							0.3	−14.0
DD							2.1	−1.1
DQ							−0.1	4.3
QQ							0.0	−0.1
Σ							324.0	−364.7
CC	O15							−129.1
CD								−11.9
CQ								−0.1
DD								−0.1
DQ								0.0
QQ								0.0
Σ								−141.2

[a]Based on integrated charges, dipoles, and quadrupoles determined at RHF/6-31G*.
[b]All values in kilocalories per mole.

that a linear change in one component of a multi-interaction situation does not necessitate a linear response. Secondly, the interactions of O_{pr} and of the carboxyl C with the CNN fragment are of the same magnitude. This observation emphasizes the general problem of *over*simplification in attempts to reduce a complicated scenario to the "essential" parts. Model building and interpretation is thus a matter of *balanced* reasoning. Some models can be eliminated because they are

Table 7. Electrostatic interaction matrix for **2**.

		N2	N3	C7	C13	O14	O15	H16
CC	C1	−21.8	13.7	1.6	47.7	−28.6	−21.2	8.9
CD		−39.7	16.7	4.9	−0.3	−12.2	1.5	0.1
CQ		12.1	−3.1	−2.3	−1.8	1.4	0.4	−0.1
DD		−8.3	3.9	−4.4	−0.2	−0.5	0.0	0.0
DQ		−3.9	3.5	0.2	−0.3	−0.2	0.0	0.0
QQ		2.3	0.2	1.5	0.0	0.0	0.0	0.0
Σ		−59.3	35.0	1.4	45.1	−40.1	−19.3	8.9
CC	N2		−95.8	−2.7	−125.7	95.0	55.4	−25.0
CD			−41.1	−6.2	−1.2	−1.1	3.6	−0.7
CQ			3.5	1.0	0.1	0.0	0.1	0.0
DD			22.6	−0.6	0.2	0.0	0.0	0.0
DQ			33.4	−0.1	−0.1	0.0	0.0	0.0
QQ			3.8	0.0	0.0	0.0	0.0	0.0
Σ			−73.7	−8.6	−126.7	93.9	59.2	−25.7
CC	N3			2.1	111.9	−92.4	−52.4	24.7
CD				3.6	17.7	−9.8	−7.9	2.5
CQ				−0.4	−0.9	−0.1	0.1	0.0
DD				0.7	−0.2	0.5	−0.2	0.0
DQ				0.4	0.1	0.0	0.0	0.0
QQ				0.0	0.0	0.0	0.0	0.0
Σ				6.4	128.6	−101.9	−60.5	27.3
CC	C7				17.1	−7.4	−7.0	2.6
CD					−19.8	−3.6	12.0	−2.7
CQ					−23.3	3.9	3.6	−0.7
DD					2.4	−0.3	0.4	−0.1
DQ					−9.3	−1.2	−0.6	0.1
QQ					−0.3	0.0	0.1	0.0
Σ					−33.3	−8.5	8.4	−0.8
CC	C13					−797.4	−685.5	242.3
CD						−269.9	−108.5	29.5
CQ						13.5	10.6	−0.7
DD						−19.3	−3.6	0.8
DQ						−11.1	−4.3	0.1
QQ						0.2	0.2	0.0
Σ						−1084.0	−790.9	272.0
CC	O14						273.2	−131.5
CD							50.1	−11.2
CQ							0.3	−0.2
DD							2.2	−0.1
DQ							0.0	0.0
QQ							0.0	0.0
Σ							325.7	−143.1
CC	O15							−302.8
CD								−40.2
CQ								−15.1
DD								−0.8
DQ								4.7
QQ								−0.1
Σ								−354.4

inconsistent with the electron density distributions, but there remains the difficult choice of selecting the best model among the ones that are consistent with the electron density distribution.

1,3-Bridging and steric interactions with the 2-position

As can be seen in Fig. 5, there occurs a bond path connecting N_α and the carbonyl-O in the molecular graph of **2**. The electron density at the bond critical point is 0.018 e au^{-3} and it is only marginally higher than the ρ_b value at the ring critical point (0.015 e au^{-3}). Equally small ρ_b values are found for the respective critical points in **1** and **3** (Table 4). What does this feature contribute to the discussion of the neighboring group interactions? Proponents of the N_α attraction model might

Table 8. Electrostatic interaction matrix for **3**.

		N2	N3	C7	C13	O14	O15
CC	C1	−12.9	7.7	1.9	33.9	−20.1	−15.0
CD		−36.7	14.3	2.0	−6.2	−10.4	3.8
CQ		11.9	−2.6	−2.6	−2.2	2.4	0.4
DD		−8.6	4.3	−8.3	0.2	−0.3	0.3
DQ		−4.8	3.7	−4.2	−0.3	−0.2	−0.1
QQ		1.9	0.2	1.9	0.0	0.0	0.0
Σ		−49.2	27.6	−9.2	25.4	−28.5	−10.6
CC	N2		−77.7	−4.8	−131.6	100.4	57.7
CD			−43.9	−4.9	−0.8	−4.7	4.7
CQ			5.1	1.6	−0.7	0.7	0.3
DD			22.3	−0.5	0.1	0.0	0.1
DQ			32.2	−0.3	−0.1	0.0	0.0
QQ			3.6	0.1	0.0	0.0	0.0
Σ			−58.3	−8.8	−133.1	96.5	62.8
CC	N3			3.5	108.2	−88.0	−50.4
CD				2.8	22.1	−15.3	−10.5
CQ				−0.6	−1.0	0.0	0.1
DD				0.5	−0.2	0.6	−0.4
DQ				0.5	0.1	0.1	−0.0
QQ				0.0	0.0	0.0	0.0
Σ				6.7	129.2	−102.6	−61.2
CC	C7				34.9	−14.9	−14.5
CD					−81.0	11.4	24.4
CQ					−3.9	0.9	2.6
DD					5.6	0.9	2.2
DQ					−0.7	−0.3	−0.9
QQ					0.0	0.0	0.0
Σ					−45.1	−1.8	13.8
CC	C13					−920.7	−920.1
CD						−186.1	−217.3
CQ						11.0	11.0
DD						−5.1	−7.1
DQ						−9.0	−10.9
QQ						0.5	0.6
Σ						−1109.4	−1143.8
CC	O14						313.3
CD							55.9
CQ							1.4
DD							2.5
DQ							−0.4
QQ							0.0
Σ							372.7

tend to be guided again by formalities and interpret the "bond path" in support of incipient bond formation between the O_{pr} donor and the electron-deficient N_α acceptor. We address this issue by analysis for consistency with the electron density distribution, by consideration of interaction lines (37) between interacting closed-shell systems, by citation of precedent for the occurrence of interaction lines between sterically interfering groups, and, finally, by citation of precedent for steric interference with the 2-position in optimizations of 1,3-bridging attractions.

The idea of incipient bond formation between the O_{pr} donor and the electron-deficient N_α acceptor is inconsistent with the electronic structures (vide supra). The N_α atom is not an acceptor but it is negatively charged. As the O_{pr} nucleophilicity increases, the negative charge of N_α *decreases* and, moreover, $q(N_\alpha)$ for **1–3** all are *less* negative than $q(N_\alpha) = -0.54$ in the parent benzenediazonium ion (14*d*). These features are not consistent with $O_{pr} \rightarrow N_\alpha$ electron donation but these electron density shifts are consistent with minimization of electron–electron repulsion between N_α and O_{pr}, that is, closed-shell or steric repulsion. The helium dimer is the simplest system for studying closed-shell interactions. Simple logic shows that there must be a "bond path" between the He atoms for *all* distances no matter whether the He atoms are far apart and essentially not bonded, in the region of the bound van-der-Waals dimer, or in the repulsive domain. The occurrence of a line connecting two attractors does not make any statement about the mode of interaction. The line just indicates "an interaction" and the better term for "bond path" is in fact "interaction line." Intramolecular interaction lines between nonconnected closed-shell systems were reported and associated with steric interactions (38).

Allyl alkali metals (39) and some of their heteroanalogues (40) prefer π-complexes in which the metal cation is located in a 1,3-bridging position between the negatively charged termini and above the best molecular plane of the allyl anion. In these cases, the distance between the metal and the C-atom at the 2-position is shorter than the contacts between the metal and the terminal carbons. The 1,3-bridging attraction model is very closely related to, and in fact can be seen as a polarity-reversed analogue of, the allyl metal bonding scenario.

Conclusion

The Bürgi–Dunitz angle of attack presents a useful concept that is easily accepted as it is in agreement with the electronic structure of carbonyls. Successful generalizations to other systems with the same bond polarity have also been described. We have argued, however, that the generalization asserted to describe the interaction of nucleophiles with diazonium ions cannot be correct. The N_α attraction model discussed by the groups of Dunitz and of Gougoutas is based on formal similarities of the C=O bond polarity and of the most commonly used Lewis structure of diazonium ions with its formally positive-charged N_α. This model relies on the assumption that the *formal* charge in the Lewis structure represents the *actual* charge distribution and the results of electronic structure analyses show that this assumption is not warranted.

The brief review of the crystallographic record on diazonium ion salts containing proximate nucleophiles shows that the distortions in their solid state structures are more fully consistent with the 1,3-bridging interaction model than with the N_α attraction model. In particular, combined analysis of solid state and of gas phase structures allows one to identify intramolecular interactions from packing effects and reveals that the intrinsic features associated with INA in diazonium ions are the CNN nonlinearity and the widening of the in-plane angles. Both of the electrostatic models can account for these features but in doing so different postulates are made concerning the electron density distribution. While the structural analysis alone cannot distinguish between the alternative interpretations, the study of the electronic structure allows one to clearly differentiate between competing inter-

Fig. 4. Electrostatic interaction energies ESI_{ij} (in kcal/mol) between pertinent pairs of atoms are shown for **1–3**. Solid (broken) arrows and negative (positive) interaction energies indicate attraction (repulsion). Values given in italics are the charge components CC_{ij} of ESI_{ij}. Atomic dipole moments are superimposed on the structures and they are directed from "o" to "•".

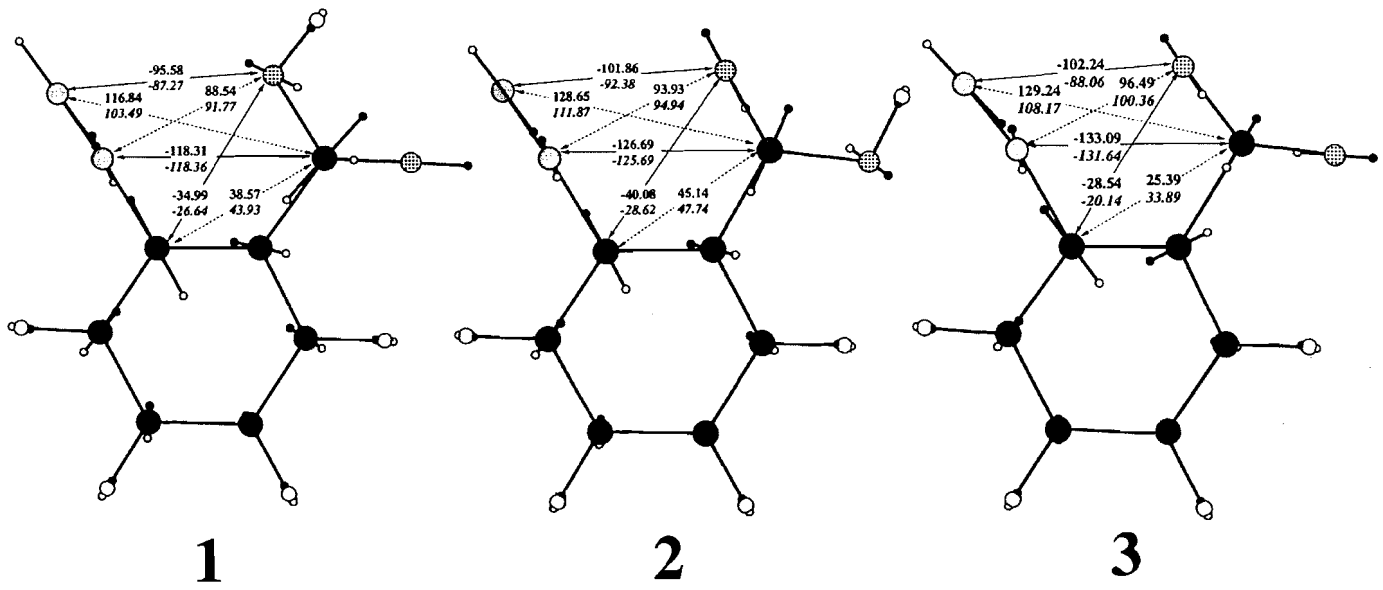

Fig. 5. The molecular graph (the collection of bond paths) of **2** is shown together with the cross sections of the zero-flux surfaces of the gradient vector field of the electron density. A "bond path" occurs between N_α and the proximate oxygen nucleophile.

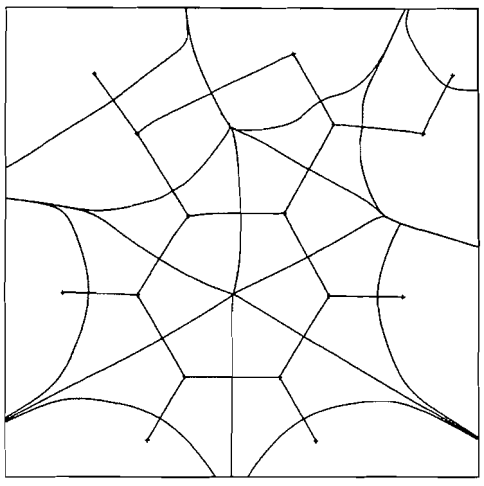

pretations of structural distortions. A method for the quantitative evaluation of electrostatic neighboring group interactions has been devised for this purpose and this ESI concept employs atomic electrical moments determined via topological electron density analysis. The results of the ESI analysis provide independent information that strongly supports the 1,3-bridging attraction model and eliminates the N_α attraction model.

The interpretation of neighboring group effects in crystal structures remains a matter of balanced reasoning. The discussion shows that some models can be eliminated because they are inconsistent with the electron density distributions, but the difficult challenge remains of identifying and selecting the best model among those that are consistent with the electron density distribution. The ESI method should prove particularly valuable for the development of electrostatic models as it is firmly based in quantum chemistry. It is hoped that these electrostatic models will allow for a better understanding of important stereochemical issues in a variety of chemical and biochemical problems.

Acknowledgment

We thank the Donors of the Petroleum Research Fund, administered by the American Chemical Society, and the Research Board as well as the Campus Computing Center of the University of Missouri for support.

References

1. (*a*) R. Glaser, C.J. Horan, E. Nelson, and M.K. Hall. J. Org. Chem. **57**, 215 (1992); (*b*) C.J. Horan, C.L. Barnes, and R. Glaser. Acta Crystallogr. Sect. C: Cryst. Struct. Commun. **C49**, 507 (1993); (*c*) Chem. Ber. **126**, 243 (1993); (*d*) C.J. Horan, P.E. Haney, C.L. Barnes, and R. Glaser. Acta Crystallogr. Sect. C: Cryst. Struct. Commun. **C49**, 1525 (1993); (*e*) R. Glaser, C.L. Mummert, C.J. Horan, and C.L. Barnes. J. Phys. Org. Chem. **6**, 201 (1993).
2. (*a*) H.-B. Bürgi, J.D. Dunitz, and E. Shefter. J. Am. Chem. Soc. **95**, 5065 (1973); (*b*) Acta Crystallogr. Sect. B: Struct. Crystallogr. Cryst. Chem. **B30**, 1517 (1974); (*c*) H.-B. Bürgi, J.D. Dunitz, J.M. Lehn, and G. Wipff. Tetrahedron, **30**, 1563 (1974); (*d*) J.D. Dunitz. Philos. Trans. R. Soc. London, Ser. B: **272**, 99 (1975); (*e*) M. Kaftory and J.D. Dunitz. Acta Crystallogr. Sect. B: Struct. Crystallogr. Cryst. Chem. **B31**, 2912 (1975); (*f*) Acta Crystallogr. Sect. B: Struct. Crystallogr. Cryst. Chem. **B31**, 2914 (1975); (*g*) Acta Crystallogr. Sect. B: Struct. Crystallogr.

Cryst. Chem. **B31**, 2917 (1975); (*h*) Acta Crystallogr. Sect. B: Struct. Crystallogr. Cryst. Chem. **B32**, 1 (1976).
3. W.B. Schweizer, G. Procter, M. Kaftory, and J.D. Dunitz. Helv. Chim. Acta, **61**, 2783 (1978).
4. K.B. Wiberg and K.E. Laidig. J. Am. Chem. Soc. **109**, 5935 (1987).
5. P.N.W. Baxter, J.A. Connor, D.C. Povey, and J.D. Wallis. J. Chem. Soc. Chem. Commun. 1135 (1991).
6. H.-B. Bürgi and V. Shklover. *In* Structure correlation. Vol. 1. *Edited by* H.-B. Bürgi and J.D. Dunitz. VCH Publishers, Inc., New York. 1994. Chap. 7.
7. G.F. Lanneau. Main Group Chem. News, **1**, 16 (1993).
8. (*a*) R.S. Glass, J.L. Broeker, and H. Firouzabadi. J. Org. Chem. **55**, 5739 (1990); (*b*) R.S. Glass, L. Adamowics, and J.L. Broeker. J. Am. Chem. Soc. **113**, 1065 (1991); (*c*) R.S. Glass. Main Group Chem. News, **2**, 4 (1994).
9. D. Britton and J.D. Dunitz. Helv. Chim. Acta, **63**, 1068 (1980).
10. (*a*) J.D. Wallis and J.D. Dunitz. J. Chem. Soc. Chem. Comm. 671 (1984); (*b*) J.D. Wallis, R.J.C. Easton, and J.D. Dunitz. Helv. Chim. Acta, **76**, 1411 (1993).
11. G.N. Lewis. *In* Valence and the structure of atoms and molecules. ACS Monogr. Ser. The Chemical Catalog Company, Inc., New York, New York, 1923.
12. R.F.W. Bader. *In* Atoms in molecules — a quantum theory. Clarendon Press, Oxford, U.K. 1990.
13. (*a*) R.F.W. Bader. Chem. Rev. **91**, 893 (1991); (*b*) Acc. Chem. Res. **18**, 9 (1985); (*c*) R.F.W. Bader, T.T. Nguyen-Dang, and Y. Tal. Rep. Prog. Phys. **44**, 893 (1981).
14. (*a*) R. Glaser. J. Phys. Chem. **93**, 7993 (1989); (*b*) J. Comput. Chem. **11**, 663 (1990); (*c*) R. Glaser, G.S.-C. Choy, and M.K. Hall. J. Am. Chem. Soc. **113**, 1109 (1991); (*d*) R. Glaser and C.J. Horan. J. Org. Chem. **60**, 7518 (1995).
15. (*a*) H. Zollinger. *In* Diazo chemistry I — Aromatic and heteroaromatic compounds. VCH, Weinheim, Germany. 1994; (*b*) *In* Diazo chemistry II — Aliphatic, inorganic, and organometallic compounds. VCH, Weinheim, Germany. 1995.
16. (*a*) R. Glaser, G.S. Chen, and C.L. Barnes. Angew. Chem. **104**, 749 (1992); Angew. Chem. Int. Ed. Engl. **31**, 740 (1992); (*b*) G.S. Chen, R. Glaser, and C.L. Barnes. J. Chem. Soc. Chem. Commun. 1530 (1993).
17. (*a*) J.Z. Gougoutas and J.J. Johnson. J. Am. Chem. Soc. **100**, 5816 (1978); (*b*) J.Z. Gougoutas. Cryst. Struct. Commun. **7**, 183 (1978); (*c*) J. Am. Chem. Soc. **101**, 5672 (1979); (*d*) Cryst. Struct. Commun. **11**, 1305 (1982).
18. M.J. Frisch, G.W. Trucks, H.B. Schlegel, P.M. Gill, P, B.G. Johnson, M.W. Wong, J.B. Foresman, M.A. Robb, M. Head-Gordon, E.S. Replogle, R. Gomperts, J.L. Andres, K. Raghavachari, J.S. Binkley, C. Gonzalez, R.L. Martin, D.J. Fox, D.J. Defrees, J. Baker, J.J.P. Stewart, and J.A. Pople. Gaussian92/DFT, Revision G.2. Gaussian Inc., Pittsburgh, Pa. 1993.
19. W.J. Hehre, L. Radom, P.v.R. Schleyer, and J.A. Pople. *In* Ab initio molecular orbital theory. John Wiley & Sons, New York. 1986.
20. F.W. Biegler-König, R.F.W. Bader, and T.-H. Tang. J. Comput. Chem. **3**, 317 (1982).
21. B. Greenberg and Y. Okaya. Acta Crystallogr. Sect. B: Struct. Crystallogr. Cryst. Chem. **B25**, 2101 (1969).
22. K. Sasvari, H. Hess, and W. Schwarz. Cryst. Struct. Commun. **11**, 781 (1982).
23. R.G. Ball and R.M. Elofson. Can. J. Chem. **63**, 332 (1985).
24. M. Cygler, M. Przybylska, and R.M. Elofson. Can. J. Chem. **60**, 2852 (1982).
25. R.M. Izatt, J.D. Lamb, C.S. Swain, J.J. Christensen, and B.L. Haymore. J. Am. Chem. Soc. **102**, 3032 (1980).
26. P. Groth. Acta Chem. Scand. Ser. A: **35**, 541 (1981).
27. R. Glaser. J. Comput. Chem. **10**, 118 (1989).
28. J.E. Carpenter and F. Weinhold. J. Mol. Struct. (Theochem), **169**, 41 (1988); (*b*) R. Arnaud. J. Comput. Chem. **15**, 1341 (1994), and references cited there.
29. R.G. Parr. Int. J. Quantum Chem. **26**, 687 (1984).
30. P.M. Walker and P.G. Mezey. J. Am. Chem. Soc. **115**, 12423 (1993).
31. R. Glaser and G.S.-C. Choy. J. Am. Chem. Soc. **115**, 2340 (1993).
32. (*a*) T. Slee. J. Am. Chem. Soc. **108**, 7541 (1986); (*b*) R.F.W. Bader, A. Larouche, C. Gatti, M.T. Carroll, P.J. MacDougall, and K.B. Wiberg. J. Chem. Phys. **87**, 1142 (1987).
33. U. Dinur and A.T. Hagler. J. Chem. Phys. **91**, 2949 (1989).
34. (*a*) S. Huzinaga, Y. Sakai, E. Miyoshi, and S. Narita. J. Chem. Phys. **93**, 3319 (1990); (*b*) S. Huzinaga and Y. Narita. Isr. J. Chem. **19**, 242 (1980).
35. D.L. Cooper and N.C.L. Stutchbury. Chem. Phys. Lett. **120**, 167 (1985).
36. R. Glaser and B.L. Harris. J. Mol. Struct. (Theochem), **255**, 45 (1992).
37. R.F.W. Bader and H. Essén. J. Chem. Phys. **80**, 1943 (1984).
38. (*a*) J. Cioslowski and S.T. Mixon. J. Am. Chem. Soc. **114**, 4382 (1992); (*b*) Can. J. Chem. **70**, 443 (1992).
39. N.J.R.v.E. Hommes, M. Bühl, and P.v.R. Schleyer. J. Organomet. Chem. **409**, 307 (1991), and references cited there.
40. (*a*) R. Glaser and A. Streitwieser. J. Org. Chem. **56**, 6612 (1991); (*b*) J. Org. Chem. **54**, 5491 (1989); (*c*) J. Am. Chem. Soc. **111**, 8799 (1989).